Journal of Alloys and Compounds 504 (2010) 413–419

Contents lists available at ScienceDirect

Journal of Alloys and Compounds

journal homepage: www.elsevier.com/locate/jallcom

# Layered Aurivillius compound: Synthesis, characterization and electrical properties

Saba Beg[a], Ahlam Al-Alas[a,*], Niyazi A.S. Al-Areqi[b]

[a] Department of Chemistry, Aligarh Muslim University, Aligarh 202002, Uttar Pradesh, India
[b] Department of Chemistry, Faculty of Applied Sciences, Taiz University, Taiz, Republic of Yemen

ARTICLE INFO

*Article history:*
Received 10 February 2010
Received in revised form 22 May 2010
Accepted 28 May 2010
Available online 8 June 2010

*Keywords:*
Sol–gel
PXRD
Thermal decomposition
AC impedance

ABSTRACT

In the present study, sol–gel citrate route was utilized to synthesize BIALVOX ($Bi_2Al_xV_{1-x}O_{5.5-x-\delta}$) in the composition range $0 \le x \le 0.20$. Powder X-ray diffraction and simultaneous thermogravimetric and differential thermal analyses confirmed that the calcination of BIALVOX xerogels is fully completed at around 500 °C after 3 h of thermal treatment. It has been found that the stabilization of highly conducting γ-phase takes place for $x \ge 0.10$. AC impedance spectroscopic investigation suggested that the charge accumulation at grain boundaries is more pronounced as compared to that at grain interiors. However, the maximum electrical conductivity ($7.73 \times 10^{-5}$ S cm$^{-1}$) was noticed for BIALVOX.13 at 300 °C. The temperature dependence of dielectric permittivity was also reported.



## 1. Introduction

BIMEVOX family of oxide-ion conductors has received much attention in recent years due to their promising applications in many practical solid devices. This family which is derived from a layered Aurivillius $Bi_4V_2O_{11}$ by partial substitution of vanadium with a metal $\left(Bi_2Me_x^{n+}V_{1-x}O_{5.5-(5-n)x/2}\right)$ exhibits the highest conductivity at moderate temperature [1–5]. The structure of the parent compound may be viewed as an intergrowth of alternating $(VO_{3.5}\square_{0.5})^{2-}$ anion deficient perovskite-like sheets and $(Bi_2O_2)^{2+}$ layers when the *c*-axis is traversed, where □ represents on oxide-ion vacancy. The high temperature phase is γ-$Bi_4V_2O_{11}$, which has a good ionic conductivity above 567 °C [1] and crystallizes in the tetragonal *I*4/*mmm* space group with the *a*-parameter close to that of the perovskite $a \sim 3.90$ Å [6]. The disordering of oxide-ion vacancies in the perovskite-like sheets as a result of substitution of vanadium with aliovalent cations is responsible for stabilization of γ-BIMEVOX to room temperature. Among the members of the BIMEVOX family, the BICUVOX.10 ($Bi_2Cu_{0.1}V_{0.9}O_{5.35}$) showed the highest conductivity at around 300 °C [2,3].

On one hand most of the BIMEVOXes were readily prepared by the conventional solid state reaction of their parent oxide powders at high temperature. Since very rare studies employed alternative low temperature routes in synthesis of some BIMEVOXes [7–11], the first aim of this paper reported here is to employ the sol–gel citrate route for synthesis of a new member of this family, with general formula $Bi_2Al_xV_{1-x}O_{5.5-x-\delta}$ (BIALVOX) for the composition range $0 \le x \le 0.20$. On other hand, AC impedance spectroscopy has become a powerful tool for the investigation of the electrical response of fast oxide-ion conducting solids. AC impedance data, performed over a wide frequency range, can be separated into two components; real or resistive part and imaginary or reactive part which are usually represented by a Nyquist diagram (or Cole–Cole plot) in terms of any of the four possible complex formalisms, the permittivity ($\varepsilon^*$), the impedance ($Z^*$), the admittance ($Y^*$), the electric modulus ($M^*$), and dielectric loss ($\tan\delta$) which are correlated to each other as follows [12]:

$$\tan\delta = \frac{\varepsilon''}{\varepsilon'} = \frac{M''}{M'} = \frac{Z'}{Z''} = \frac{Y'}{Y''} \quad (1)$$

The inter-particle interactions such as grain and grain boundary effects are easily determined with the help of the complex impedance formalism. The Bouwkamp's formalism of impedance [13] is given by:

$$Z*(\omega) = \frac{R}{1 + RB(j\omega)^n}, \quad j = \sqrt{-1} \quad (2)$$

where *R* is the intercept of the curve at high frequency with real axis. The parameters *Y* and *n* are extracted by theoretical fitting of data.

It is worthwhile to note that detailed information on AC impedance behaviour in BIMEVOXes is rare. Therefore, the second aim of this paper will focus on the impedance spectroscopic inves-

* Corresponding author. Tel.: +91 9997385220/9897283959.
*E-mail address:* ahlamalalas@gmail.com (A. Al-Alas).

0925-8388/$ – see front matter. 
doi:10.1016/j.jallcom.2010.05.133

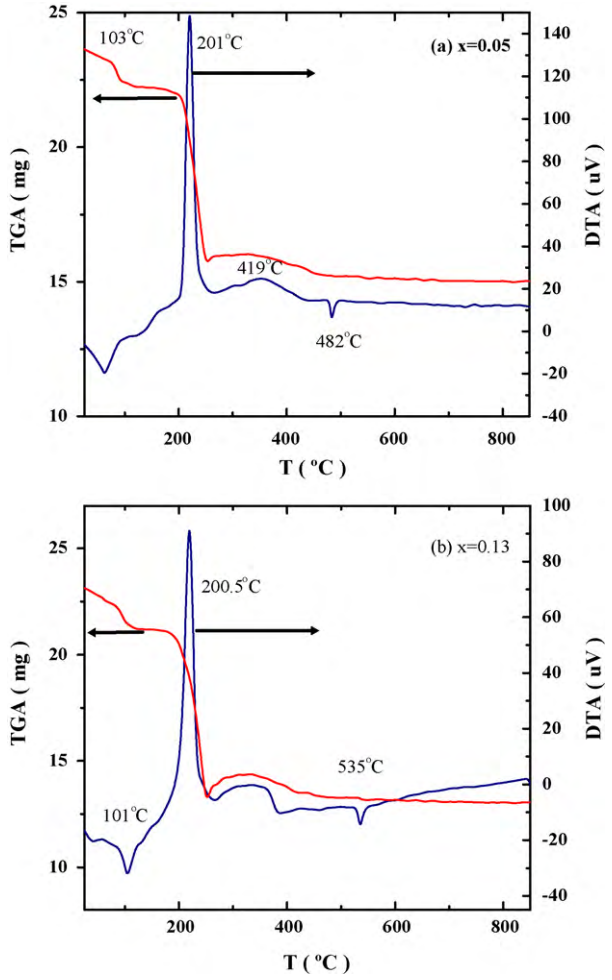


**Fig. 1.** TGA–DTA curves of BIALVOX xerogels for various compositions: (a) BIALVOX.05 and (b) BIALVOX.13.

tigations on the BIALVOX system in order to correlate the structural and electrical properties.

## 2. Experimental

Analytical grade $Bi(NO_3)_3{\cdot}5H_2O$, $NH_4VO_3$ and $Al(NO_3)_3{\cdot}9H_2O$ were used as starting materials. Stock solutions of the starting materials (1 M) were prepared by dissolving an accurately weighed amount of corresponding material in deionized water. Stock solution of citric acid (2 M) used as complexant agent was also prepared. Another solution containing $NH_3$ (2 M) was used to adjust the pH of sol mixture. The starting material solutions were mixed in a molar ratio of $2{:}x{:}(1-x) = Bi^{3+}{:}Al^{3+}{:}V^{5+}$. Citric acid solution was then added to each mixture to form the complexation solution. The ratio of citric acid to total metal ions was set at 1.5:1. The pH of resulting solutions was then adjusted to ~7 by the addition of ammonia solution. The solution was heated at 80 °C under vigorous stirring for 1 h to form a transparent gel. The xerogel (precursor metal complex) was then obtained by drying the resulting gel on air at 90 °C for 24 h.

The xerogels were thoroughly mixed in an agate mortar for further homogenization and thereafter calcinated in a muffle furnace at 650 °C for 3 h. The BINAVOX powders were pelletized into a cylinderical shape with constant dimensions (24 mm in diameter × 1 mm in thickness) under isostatic pressure of 510 MPa (Spectralab SL-89). The pellets were then sintered on air at 800 °C for 5 h.

The thermal decomposition of the xerogel was investigated by simultaneous thermogravimetric analysis and differential thermal analysis (TGA–DTA) using a Perkin Elmer thermal analyzer up to 1000 °C at a heating rate of 10 °C $min^{-1}$ with an air flow rate of 30 ml $min^{-1}$. α-Alumina was used as a reference material.

The thermal decomposition of xerogel was also followed by powder X-ray diffraction data. The PXRD patterns were recorded for xerogel powders calcinated at different temperatures using a Rigaku/Max-B X-ray diffractometer employing Ni-filtered CuKα radiation (λ = 1.54060 Å) operated with Bragg–Brentano geometry in the range $5^\circ \le 2\theta \le 90^\circ$ with an increment of 0.05° at scantime of 0.6 s/increment.

PXRD analyses were also employed to characterize the phase structure of BIALVOX system at room temperature as a function of composition. The PXRD patterns were collected for various compositions after calcination at 650 °C for 3 h. The unit cell dimensions were refined on POWDERX software program.

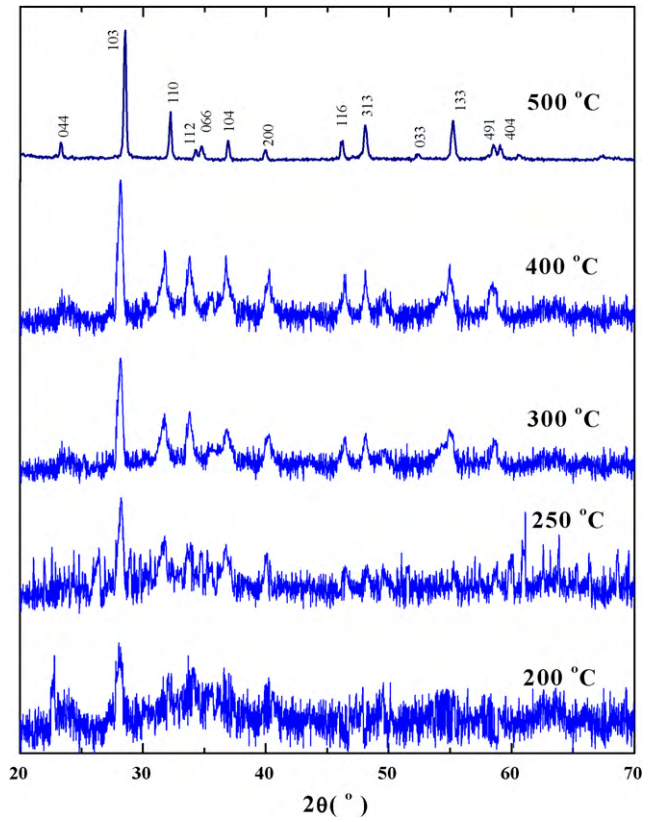


**Fig. 2.** PXRD patterns of BIALVOX.10 xerogel calcinated at different temperatures for 3 h.

AC impedance measurements were carried out on a Solarton 1260 impedance analyzer operated in the frequency range of 5 Hz–6.5 MHz with an AC signal of ~50 mV. The sintered pellets were made conducting by applying chemically pure silver paste, used as electrodes on both flat surfaces of the pellets and were re-sintered at 700 °C for 5 h. The experiments were run in air in the temperature range of 200–840 °C with an increment of 20 °C.

## 3. Results and discussion

### 3.1. Structural characterization

TGA–DTA curves for xerogels are presented in Fig. 1, which exhibit a broad endothermic peak around ~100 °C and an exothermic peak started from ~190 and extending up to ~420 °C. The TGA curves show two steps in the total weight loss. The first step in the TGA curves starts from room temperature to ~115 °C with weight loss of ~7.5%. This corresponds to the endothermic peak in DTA curves and is attributed to the loss of residual ammonia and water as well as the elimination of free ammonium citrate [14,15]. The major weight loss in the second step (~34%) occurs from ~190 to ~420 °C and correlates with the exothermic peak in DTA curves. The temperature region of the second step can be recognized into two subregions according to the type of decomposition process. The first subregion extending from ~190 to ~225 °C, corresponding to the sharp exothermic peak, is due to the partial decomposition of the precursor metal complex, while the final one extending up to ~420 °C is mainly associated with the decarbonization reaction of residual citrate which is usually accompanied with an exothermic curvature [16,17]. It is worthwhile to point that the heat flow per unit mass associated with the sharp exothermic peak in DTA curves decreases significantly

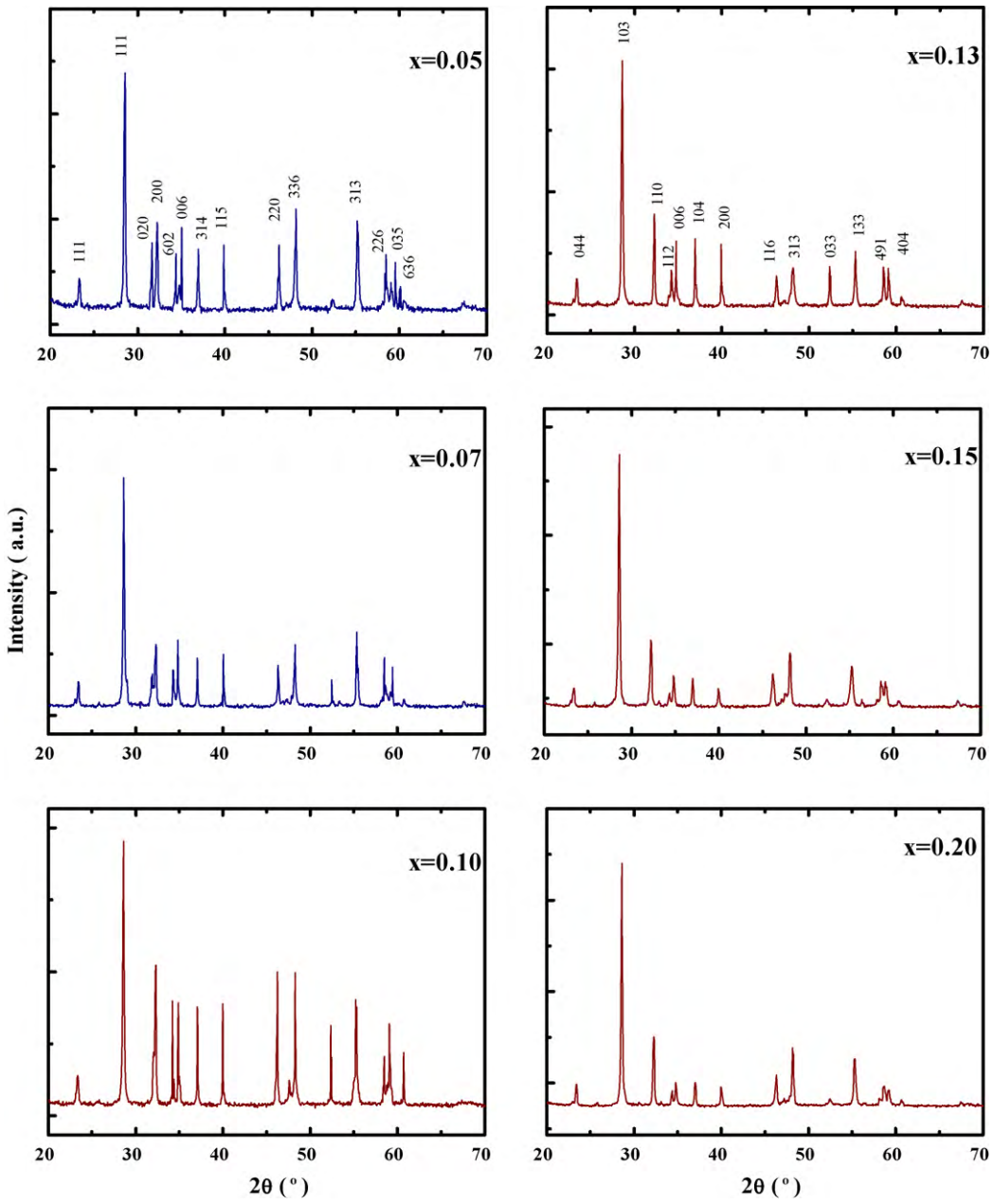


**Fig. 3.** PXRD patterns of BIALVOX system for various compositions after calcinations at 650 °C for 3 h.

with increasing Al content in the xerogels (e.g. from $-277.3\,J\,g^{-1}$ for $x = 0.05$ to $-195.9\,J\,g^{-1}$ for $x = 0.13$). This trend in the heat flow suggests that the stability of the precursor metal complex against the thermal decomposition increases with increasing dopant concentration.

Furthermore, the DTA curves exhibit small endothermic effects at temperatures above 456 °C, corresponding to no mass loss, which can be assigned to phase transition changes occurring in BIMEVOX materials [18,19]. However, single endothermic peaks noticed at 482 °C for BIALVOX.05 (Fig. 2a), respectively, are correlated with $\beta \rightarrow \gamma$ transition, while those noticed for BIALVOX.13 (Fig. 2b) at 535 °C, respectively, are attributed to the occurrence of an order–disorder, $\gamma' \rightarrow \gamma$ transition. The heat flow per unit mass due to $\beta \rightarrow \gamma$ and $\gamma' \rightarrow \gamma$ transitions in the BIALVOX system is found to be relatively higher than that reported for the BIHFVOX system [19]. This can be correlated with the fact that the phase stability is decreased with increasing ionic radius of dopant cation.

The thermal decomposition of BIALVOX xerogels has been further examined by powder X-ray diffraction data. The PXRD patterns of BIALVOX.10 xerogel calcinated at different temperatures are presented in Fig. 2. The PXRD pattern becomes more obvious as the calcination temperature increases. This can be attributed to the partial decomposition of citrate precursor. At 400 °C, the broad diffraction peaks exhibit *I*4/*mmm* symmetry, characteristic to the tetragonal phase. This is in perfect agreement with TGA–DTA results. It can be seen that the broadening of the peaks gradually decreases with increasing temperature, signifying the increase in crystalline particles with increasing temperature [20]. However, the temperature around 500 °C can be considered quite sufficient to achieve the fully tetragonal crystalline structure, as clearly evidenced by the appearance of smooth diffraction pattern at this temperature.

PXRD patterns of BIALVOX system for various compositions calcinated at 650 °C are exhibited in Fig. 3. The β- and γ-phases can obviously be distinguished by PXRD in the $2\theta$ range ≈31–33°. The

**Table 1**
Refined unit cell dimensions for different compositions of the BIALVOX system.

| $x$ | $a$ (Å) | $b$ (Å) | $c$ (Å) | $V$ (Å$^3$) | Phase model |
|---|---|---|---|---|---|
| 0.05 | 5.521 | 5.544 | 15.369 | 470.42 | β |
| 0.07 | 5.533 | 5.547 | 15.416 | 473.14 | β |
| 0.10 | 3.911 | – | 15.420 | 235.86 | γ |
| 0.13 | 3.918 | – | 15.423 | 236.75 | γ |
| 0.15 | 3.921 | – | 15.425 | 237.15 | γ |
| 0.20 | 3.920 | – | 15.527 | 237.06 | γ |

orthorhombic β-phase is described by the presence of a doublet sublattice peak ascribed as (0 2 0) and (2 0 0) at $2\theta \approx 32^\circ$, while the tetragonal γ-phase is assigned to a singlet sublattice peak (1 1 0) at $2\theta \approx 32.5^\circ$ [18,21,22]. Accordingly, compositions with $x \leq 0.07$ belong to β-type with space group, *Aba*2. However, the stabilization of tetragonal γ-phase takes place for compositions $x \geq 0.10$. Contrary to what have been noticed for γ-BICEVOX [22], the diffraction peaks for γ-BIALVOX at $2\theta \approx 54.5$–$60^\circ$ could effectively be indexed as (1 3 3), (4 9 1) and (4 0 4), which suggest the higher tetragonal symmetry in Al-substituted system.

Table 1 summarizes the unit cell dimensions evaluated by the refinement of the whole diffraction profile. It is interesting to point that the refinement has been performed using the mean orthorhombic cell [23]. Generally, the *c*-axis dimension gradually increases as Al-concentration increases. This increasing trend in the *c*-dimension correlates with the substitution of $V^{5+}$ with smaller effective ionic radius (0.54 Å) by the larger $Al^{3+}$ (0.68 Å) in the $Bi_4V_2O_{11}$ lattice structure [24].

### 3.2. AC impedance spectroscopy

The complex impedance data for BIALVOX.13 taken at different temperatures are shown in Fig. 4. It can be noted that below ~460 °C, two semicircular arcs are obviously observed; a large arc which is usually situated in the high-frequency region, is assigned to the grain interior contribution, while the low-frequency arc represents the small contribution of grain boundaries. There is also an additional contribution from the electrode–electrolyte interface, typified in the existence of an inclined spur at the lowest frequencies which has been entirely extracted from the impedance data in order to investigate the impedance response of the only BIALVOX electrolyte. Above ~460 °C, the semicircular arcs disappear rapidly with increasing temperature and the impedance data are seen as the inclined spur at an angle of ~50°, due to the limited experimental frequency range employed and to the fast increase in the time constant of impedance response with increasing temperature.

According to the brick layer model [25–27], the impedance response of BIALVOX electrolyte is modeled as a series association of parallel ($R_g$–$CPE_g$) and ($R_{gb}$–$CPE_{gb}$) circuits for grain interior and grain boundary contributions, respectively. The constant phase element ($CPE_i$) is defined by two characteristic parameters; the factor B and $n$ ($-1 < n < 1$) according to the relation:

$$Y(\omega) = B(j\omega)^n \tag{3}$$

The impedance spectra were fitted by a non-linear least-squares using Zview software. $\chi^2$ and WSS methods were taken into account to test the validity of fitting procedure. Total resistance ($R_t$) of the material is a sum of the grain and grain boundary resistances:

$$R_t = R_g + R_{gb} \tag{4}$$

where $R_g$ and $R_{gb}$ can be obtained from the intercept of the grain and grain boundary arcs, respectively, with the resistive part of complex impedance plot ($Z'$-axis). The capacitances ($C_i$) and relaxation times ($\tau_i$) are computed using Eqs. (5) and (6):

$$C_i = \left[B_i \cdot R_i^{(1-n_i)}\right]^{1/n_i} \tag{5}$$

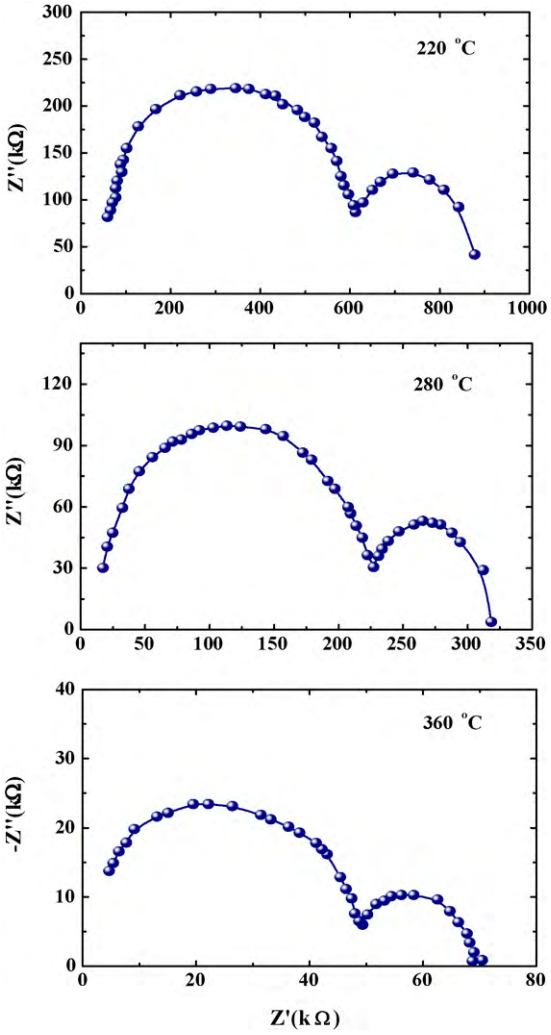


**Fig. 4.** Complex impedance plots for BIALVOX.13 at different temperatures.

$$\tau_i = \frac{1}{2\pi f_{\max,i}} \tag{6}$$

where $f_{\max,i}$ is the applied frequency in Hz at the maximum of either grain or grain boundary arcs. The equivalent circuit parameters estimated from the complex impedance data presented in Fig. 5 are summarized in Table 2. They have been determined as a function of temperature. On increasing the temperature, both $R_g$ and $R_{gb}$ decrease exponentially in the behaviour similar to the variation of $R_t$ with temperature. This is attributed to the thermally activated conduction processes expected with BIALVOX system. In most cases, at ambient temperature, the values of $R_g$ are much larger than that of $R_{gb}$, indicating that the contribution of the grain interior to the total ionic conduction is much more pronounced compared to that of grain boundaries [28,29], due to which the oxide-ion vacancies become more mobile in the grain boundaries. It is found that the frequency at arc maxima shifts towards a high-frequency side which can also be confirmed by the variation of $\tau_g$ and $\tau_{gb}$ as a function of temperature. Furthermore, the values of $C_{gb}$ are higher than that of $C_g$ by nearly two orders of magnitude at the same temperature. Moreover, the increase in $C_{gb}$ value with increasing temperature generally suggests that the charge carrier accumulation at grain boundaries is more pronounced as compared to that at the grain interiors.

**Table 2**
Values of the equivalent circuit parameters deduced from the impedance spectra for BIALVOX.13 at various temperatures.

| $T$ (°C) | $R_g$ (kΩ) | $C_g$ (F) | $\tau_g$ (s) | $R_{gb}$ (kΩ) | $C_{gb}$ (F) | $\tau_{gb}$ (s) | $R_t$ (kΩ) | $\chi^2$ | WSS |
|---|---|---|---|---|---|---|---|---|---|
| 220 | 552.90 | $1.10 \times 10^{-12}$ | $6.07 \times 10^{-7}$ | 265.80 | $7.94 \times 10^{-11}$ | $2.11 \times 10^{-5}$ | 818.70 | $1.5 \times 10^{-3}$ | 0.174 |
| 260 | 276.55 | $1.85 \times 10^{-12}$ | $5.13 \times 10^{-7}$ | 135.49 | $1.36 \times 10^{-10}$ | $1.84 \times 10^{-5}$ | 400.04 | $1.3 \times 10^{-3}$ | 0.158 |
| 280 | 210.01 | $2.24 \times 10^{-12}$ | $4.71 \times 10^{-7}$ | 91.21 | $1.68 \times 10^{-10}$ | $1.53 \times 10^{-5}$ | 301.22 | $1.7 \times 10^{-3}$ | 0.166 |
| 320 | 91.58 | $5.69 \times 10^{-12}$ | $4.21 \times 10^{-7}$ | 38.01 | $2.76 \times 10^{-10}$ | $1.05 \times 10^{-5}$ | 129.59 | $1.3 \times 10^{-3}$ | 0.127 |
| 360 | 44.70 | $8.10 \times 10^{-12}$ | $3.62 \times 10^{-7}$ | 19.37 | $4.47 \times 10^{-10}$ | $8.66 \times 10^{-6}$ | 64.07 | $1.6 \times 10^{-3}$ | 0.139 |
| 400 | 18.95 | $1.61 \times 10^{-11}$ | $3.05 \times 10^{-7}$ | 9.41 | $7.35 \times 10^{-10}$ | $6.92 \times 10^{-6}$ | 28.36 | $1.5 \times 10^{-3}$ | 0.161 |

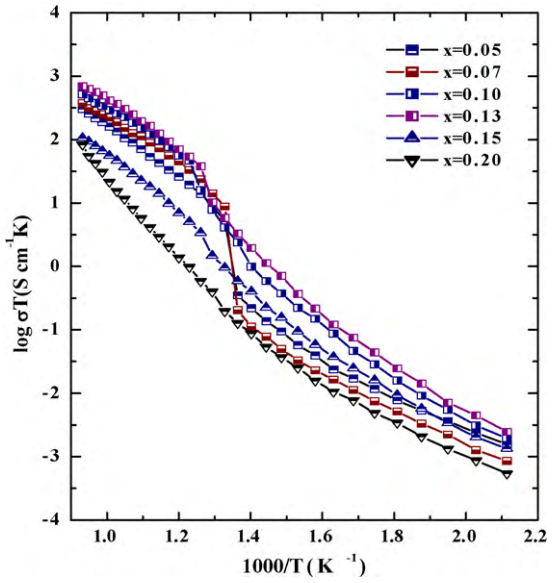


**Fig. 5.** Temperature dependence of electrical conductivity for BIALVOX system vs. composition.

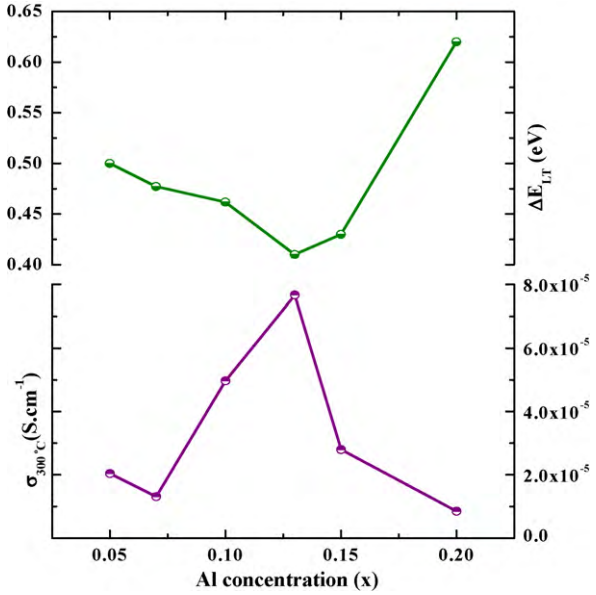


**Fig. 6.** Low temperature conductivity and activation energy for BIALVOX system vs. composition.

The electrical conductivity was deduced from the AC impedance data as follows:

$$\sigma = \left(\frac{1}{R_t}\right)\left(\frac{L}{A}\right) \quad (7)$$

where $L$ is the distance between the electrodes with flat surface area of $A$. Temperature dependence of electrical conductivity was presented in the form of $\log \sigma T$ vs. $1000/T$, following Arrhenius dependence:

$$\sigma T = A \exp\left(\frac{-\Delta E_a}{kT}\right) \quad (8)$$

Fig. 5 shows the temperature dependence of electrical conductivity of the BIALVOX system for various compositions. For compositions with $x \leq 0.07$, where the β-polymorph is stabilized at room temperature, the variation of conductivity with temperature exhibits an abrupt change in the plot (non-Arrhenius behaviours) at temperatures corresponding to the endothermic peaks detected in DTA curves. Thus, these plots can be visualized as two obvious domains, located in low and high temperature regions, assigned to the conductivity behaviour of β- and γ-phases, respectively.

For compositions $0.10 \leq x \geq 0.15$ with stabilized tetragonal phase, there is a subtle change in the Arrhenius plots, which is associated with the $\gamma' \rightarrow \gamma$ transition [18,23]. It is also interesting to note that such subtle change, resulting from a rapid disordering of oxygen atoms in the perovskite-like sheets becomes discrete on increasing dopant concentration, so that two linear domains assigned to the γ′- and γ-phases could not be recognized. There is merely a point in the Arrhenius plot at which the activation energy changes [30–32] e.g. at 520 °C which was exhibited by BIALVOX.20.

The activation energy was computed from Eq. (8) using a linear least-squares fitting in the temperature ranges 200–460 and 560–800 °C for low and high temperature activation energies ($\Delta E_{LT}$ and $\Delta E_{HT}$), respectively. The variation in low temperature conductivity ($\sigma_{300}$) and low temperature activation energy as a function of Al concentration is presented in Fig. 6. It is observed that the low temperature activation energy shows a gradual decrease with

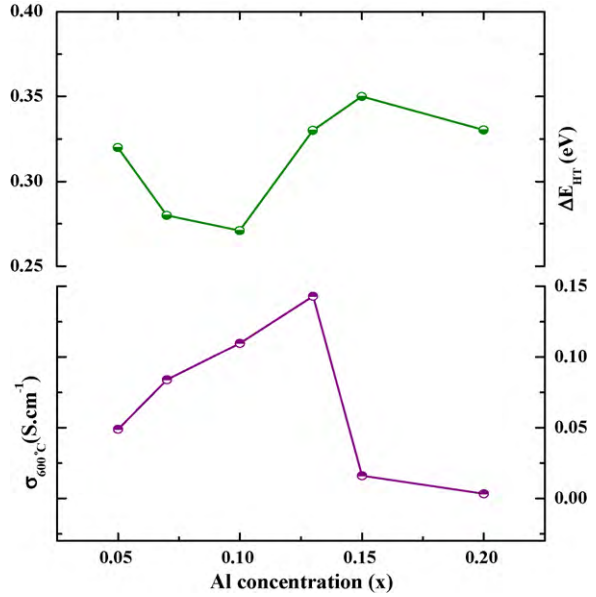


**Fig. 7.** High temperature conductivity and activation energy for BIALVOX system vs. composition.

**Table 3**
Comparison of the low temperature conductivity for BIALVOX.13 with those reported for some important BIMEVOXes.

| BIMEVOX | ME | $T$ (°C) | Phase | Conductivity (S cm$^{-1}$) | Ref. |
|---|---|---|---|---|---|
| BIALVOX.13 | $Al^{3+}$ | 300 | γ′ | $7.73 \times 10^{-5}$ | In this work |
| BICUVOX.05 | $Cu^{2+}$ | 300 | β | $1.2 \times 10^{-5}$ | [2] |
| BICUVOX.10 | $Cu^{2+}$ | 237 | γ′ | $\sim 1 \times 10^{-3}$ | [3] |
| BICDVOX.10 | $Cd^{2+}$ | 300 | γ′ | $1.17 \times 10^{-5}$ | [18] |
| BILAVOX.10 | $La^{3+}$ | 300 | γ′ | $1.4 \times 10^{-4}$ | [34] |
| BIGDVOX.10 | $Gd^{3+}$ | 300 | β | $2.27 \times 10^{-4}$ | [35] |
| BICEVOX.15 | $Ce^{4+}$ | 320 | γ′ | $1.90 \times 10^{-5}$ | [22] |
| BIHFVOX.15 | $Hf^{4+}$ | 340 | γ′ | $1.48 \times 10^{-5}$ | [19] |

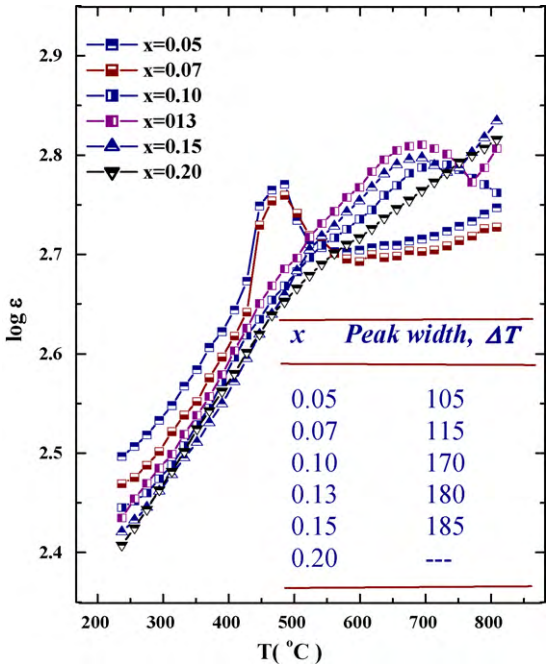


**Fig. 8.** Temperature dependence of dielectric permittivity for BIALVOX system vs. composition. Inset shows the variation in dielectric peak width as a function of $x$.

increasing Al content up to $x = 0.13$ as a minimum is observed (~0.42 eV) which couples with a maximum in the conductivity taken at 300 °C ($\sigma_{300} \sim 7.73 \times 10^{-5}$ S cm$^{-1}$). The initial decrease in $\Delta E_{LT}$ with increasing value of $x$ until the minimum at $x = 0.13$ is due to the increase in vacancy concentration in equatorial planes of the perovskite-like sheets. A sudden increase in $\Delta E_{LT}$ as well as the decrease in low temperature conductivity as a function of Al concentration beyond $x = 0.13$, are correlated with defect trapping effects which have a negative contribution to the magnitude of conductivity. It is worthwhile to mention that an increase in vanadium reduction, the defect trapping effects are increased, leading to lower overall conductivities and higher activation energies [33]. Table 3 compares the maximum conductivity for BIALVOX.13 at 300 °C with those reported for some important BIMEVOXes at lower temperatures. It can be noted that the maximum conductivity exhibited BIMEVOXes depends on neither the effective ionic radius nor the charge of dopant metal ion. Study of the defect structure in γ-phase [36,37] has shown that the conduction mechanism in such systems is influenced by two factors. The first factor is the maximum vacancy concentration in the equatorial planes of vanadate layers. The second one is the capability of vanadate structure to form a five-coordinate intermediate due to the fast vacancy exchange and polarization of $6s^2$Bi lone pairs. Contrary to what have been reported for most BIMEVOXes [2,22,31,32], the high temperature conductivity ($\sigma_{600}$) does not show an exponential decay with increasing value of $x$ (Fig. 7 ). Instead, it exhibits a maximum conductivity for $x = 0.13$ ($\sigma_{600} \sim 0.143$ S cm$^{-1}$ and $\Delta E_{HT} \sim 0.36$ eV).

The dielectric permittivity of the BIALVOX system was obtained using the relation below:

$$\varepsilon_{6.5\ \mathrm{MHz}} = \left(\frac{C_p}{\varepsilon_o}\right)\left(\frac{L}{A}\right) \quad (9)$$

where $C_p$ is the value of capacitance, corresponding to the real part of complex impedance, measured at 6.5 MHz and $\varepsilon_o$ is a permittivity of vacuum (~$8.854 \times 10^{-14}$ F cm$^{-1}$). The temperature dependence of dielectric permittivity of the BIALVOX system for various composition is represented as ($\log \varepsilon$ vs. $T$) plot as shown in Fig. 8. It is observed that the dielectric permittivity generally increases with increasing temperature, reaches a maximum, corresponding to the phase change and then decreases. It is also found that the broadening of dielectric peaks for compositions with stabilized γ-phase increases with increasing value of $x$.

## 4. Conclusions

In the present work, standard sol–gel citrate method has been employed for synthesis of the BIALVOX oxide-ion conductor. The structural characterization elucidated that the xerogels with different compositions were entirely calcinated at temperatures around 500 °C. AC impedance spectroscopy gave detailed information on electrical conductivity and dielectric permittivity. In general, the BIALVOX system exhibited considerable features, comparable to other studied BIMEVOXes.

## Acknowledgements

We are highly obliged to Professor Kamaluddin, Chairman of Chemistry Department, I.I.T., Roorkee, for his useful discussion. We would also like to express our deepest gratitude to Taiz University, Taiz, Republic of Yemen, for granting research scholarships.

## References

[1] F. Abraham, M.F. Debreuille-Gresse, G. Mairesse, G. Nowogrocki, Solid State Ionics 28–30 (1988) 529.
[2] F. Abraham, J.C. Boivin, G. Mairesse, G. Nowogrocki, Solid State Ionics 40–41 (1990) 934.
[3] E. Pernot, M. Anne, M. Bacmann, P. Strobel, J. Fouletier, R.N. Vannier, G. Mairesse, F. Abraham, G. Nowogrocki, Solid State Ionics 70–71 (1994) 259.
[4] O. Joubert, A. Jouanneaux, M. Ganne, R.N. Vannier, G. Mairesse, Solid State Ionics 73 (1994) 309.
[5] G. Mairesse, C. R. Acad. Sci. Paris t 2, Ser. IIc (1999) 651.
[6] S. Lazure, Ch. Vernochet, R.N. Vannier, G. Nowogrocki, G. Mairesse, Solid State Ionics 90 (1996) 117.
[7] A.K. Bhattacharya, K.K. Mallick, P.A. Thomas, Solid State Commun. 91 (1994) 357.
[8] K. Shantha, K.B.R. Varma, J. Mater. Res. 14 (1999) 4651.
[9] J.W. Pell, K.M. Delak, H.-C. Zur Loye, Chem. Mater. 19 (1998) 1764.
[10] J.W. Pell, R.C.Y. Auyeung, D.B. Chrisey, H.-C. Zur Loye, Thin Solid Films 300 (1997) 154.
[11] B. Vaidhyanathan, K. Balaji, K.J. Rao, Chem. Mater. 10 (1998) 3400.
[12] R. Gerhard, J. Phys. Chem. Solids 55 (1994) 1491.
[13] M.A. de Lima Nobre, S. Lanfredi, Mater. Res. 2 (2003) 151.
[14] P. Courty, H. Ajot, C. Marcilly, Powder Technol. 7 (1973) 21.
[15] M.S.G. Bayathoun, F.R. Sale, Mater. Sci. 17 (1982) 2757.
[16] S. Doeuff, M. Henry, C. Sanchez, Mater. Res. Bull. 25 (1990) 1519.
[17] J.C. Yu, J. Yu, W. Ho, Z. Jiang, L. Zhang, Chem. Mater. 14 (2002) 3808.

[18] S. Beg, N.S.A. Al-Areqi, S. Haneef, Solid State Ionics 179 (2008) 2260.
[19] S. Beg, N.A.S. Al-Areqi, A. Al-Alas, J. Alloy Compd. 479 (2009) 107–112.
[20] R.A. Rocha, E.N.S. Muccillo, Mater. Res. Bull. 38 (2003) 1979.
[21] C.J. Watson, A. Coasts, D.C. Sinclair, J. Mater. Chem. 7 (1997) 2091.
[22] S. Beg, N.A.S. Al-Areqi, Philos. Mag. 89 (2009) 1279.
[23] N.A.S. Al-Areqi, S. Beg, Mater. Chem. Phys. 115 (2009) 5.
[24] R.D. Shannon, C.T. Prewitt, Acta Crystallogr. B 25 (1969) 925.
[25] F. Fleig, J. Maier, J. Eur. Ceram. Soc. 19 (1999) 693.
[26] F. Fleig, J. Maier, J. Electrochem. Soc. 145 (1998) 2081.
[27] M. Guillodo, J. Fouletier, L. Dessemond, P. Del Gallo, J. Eur. Ceram. Soc. 21 (2001) 2331.
[28] M.H. Payadar, A.M. Hadian, K. Shiamnoe, N. Yamazoe, J. Eur. Ceram. Soc. 21 (2001) 1825.
[29] M.J. Godinho, P.R. Bueno, M.O. Orlandi, E.R. Leite, E. Longo, Mater. Lett. 57 (2003) 2540.
[30] O. Joubert, M. Ganne, R.N. Vannier, G. Mairesse, Solid State Ionics 83 (1996) 199–207.
[31] F. Krok, I. Abrahams, A. Zadrozna, M. Malys, W. Bogusz, J.A.G. Nelstrop, A.J. Bush, Solid State Ionics 119 (1999) 139–144.
[32] W. Wrobel, I. Abrahams, F. Krok, A. Kozanecka, S.C.M. Chan, M. Malys, W. Bogysz, J.R. Dygas, Solid State Ionics 176 (2005) 1731.
[33] I. Abrahams, F. Krok, M. Malys, A.J. Bush, J. Mater. Sci. 36 (2001) 1099.
[34] C.K. Lee, A.R. West, Solid State Ionics 86–88 (1996) 235.
[35] C.K. Lee, C.S. Ong, Solid State Ionics 117 (1999) 301.
[36] I. Abrahams, F. Krok, Solid State Ionics 157 (2003) 139.
[37] I. Abrahams, F. Krok, J. Mater. Chem. 12 (2002) 3351.